Appl. Phys. A 80, 1419–1423 (2005)
DOI: 10.1007/s00339-004-3040-0

Applied Physics A
Materials Science & Processing

W. YANG[1]
L. ZHANG[2]
Z. XIE[1,✉]
J. LI[1]
H. MIAO[1]
L. AN[2,3]

Growth and optical properties of ultra-long single-crystalline α-Si_3N_4 nanobelts

[1] State Key Lab of New Ceramics and Fine Processing, Tsinghua University, Beijing 100084, P.R. China
[2] Laboratory of Excited State Processes, Changchun Institute of Optics, Fine Mechanics and Physics, Chinese Academy of Sciences, Changchun, P.R. China
[3] Advanced Materials Processing and Analysis Center (AMPAC), University of Central Florida, Orlando, FL 32816, USA

Received: 19 June 2004/Accepted version: 26 August 2004
Published online: 3 November 2004 •

ABSTRACT Ultra-long single-crystalline α-Si_3N_4 nanobelts were synthesized by catalyst-assisted crystallization of polymer-derived amorphous silicon carbonitride (SiCN). The obtained nanobelts were characterized using X-ray diffraction, scanning electron microscopy, high-resolution transmission electron microscopy and selected-area electron diffraction. The results revealed that the α-Si_3N_4 nanobelts are 20 to 40 nm in thickness, 400–600 nm in width and a few hundreds of micrometers to several millimeters in length, and grow along either the [011] or the [100] direction. Intense visible photoluminescence was observed over a spectrum ranging from 1.65 to 3.01 eV, which can be attributed to defects in the α-Si_3N_4 structure.

PACS 81.07.-b; 78.67.-n; 81.05.Je

1 Introduction

Recently, synthesis of one-dimensional nanostructured silicon nitride has attracted great attention since it is potentially important for applications in electronic/optical nanodevices and nanocomposites for harsh environments. Si_3N_4 nanowires have been synthesized by either confined reaction using carbon nanotubes as templates [1] or reacting Si and/or SiO_2 with N_2 by heat treatment or combustion with or without catalysts [2–5]. Zhang et al. demonstrated that Si_3N_4 nanowires possess much higher bending strength than the bulk [6]. Chen et al. synthesized well-aligned silicon nitride nanocones on Si substrates by plasma-assisted hot-filament chemical vapor deposition [7]. More recently, silicon nitride of belt-like morphology has also been synthesized in both nanoscale [8] and micrometer scales [9, 10] via vapor–solid thermal reaction and thermal decomposition of nitridation. Silicon nitrides could be excellent host materials in terms of mechanical strength, thermal/chemical stability and high dopant concentration [11, 12], similar to the III-N compounds (such as GaN and AlN) that are used to grow quantum-well structures for obtaining blue lasers. Previous studies of the optical properties of silicon nitride primarily focused on non-stoichiometric amorphous SiN_x thin films [12–15]. These studies suggested that the optical emission of the silicon nitrides could be attributed to the inherent point defects associated with amorphous SiN_x, such as Si−Si, N−N and Si and N dangling bonds. Few studies of the optical properties of single-crystalline Si_3N_4 have been reported. Munakata et al. studied the absorption behavior of Al-doped β-Si_3N_4 single crystal [11], and reported the existence of a mid-gap level of ∼ 2.4 eV associated with Al impurity. Yin et al. reported a broad optical emission from α-Si_3N_4 nanobelts [8].

In this communication we report the synthesis and optical emission of ultra-long single-crystalline α-Si_3N_4 nanobelts. The nanobelts were prepared using a novel catalyst-assisted crystallization of amorphous SiCN synthesized by thermal decomposition of a polysilazane polymeric precursor. A similar technique has been used to synthesize silicon carbide/nitride nanostructures [16–18]. In this paper, the process has been optimized so that single-phase α-Si_3N_4 single-crystalline nanobelts were obtained. The crystalline structure and morphology of the nanobelts were characterized using X-ray diffraction (XRD), scanning electron microscopy (SEM), transmission electron microscopy (TEM) and selected-area electron diffraction (SAED). The photoluminescence (PL) of the nanobelts has been recorded under excitation of a 325-nm HeCd laser at room temperature.

2 Experimental

Polyureasilazane (Ceraset™, Kion Corporation, USA) was used as the starting precursor. The as-received Ceraset, which is liquid at room temperature, was first solidified by heat treatment at 260 °C for 0.5 h. The solidification was due to the cross-linking reaction of C=CH_2 and Si−H bonds within the individual Ceraset molecule [19]. The obtained solid was then crushed into fine powder by high-energy ball milling for 24 h. 3 wt. % $FeCl_2$ powder (Beijing Bei Hua Fine Chemicals Company Ltd., Beijing, China) was added during ball milling as a catalyst. The powder mixture was then placed in a high-purity alumina crucible and pyrolyzed in a conventional furnace with a graphite resistance under flowing ultra-high-purity nitrogen of 0.1 MPa. The powder mixture was heated to 1300 °C at 10 °C/min and held there for 2 h followed by furnace cooling. The morphology, structure and composition of the pyrolysis products were characterized using SEM (JSM-6301, JEOL, Japan), XRD (Automated D/Max-RB, Rigaku, Japan) with Cu Kα radiation

✉ Fax: +86-10-6279-4603, E-mail: xzp@mail.tsinghua.edu.cn

($\lambda = 1.54178$ Å) and high-resolution transmission electron microscopy (HRTEM) (JEOL-2010F, Japan) equipped with energy-dispersive spectroscopy (EDS). The experiments were also performed on the samples without $FeCl_2$ additives for comparison.

In order to measure their photoluminescence, an attempt has been made to separate the nanobelts from remaining amorphous matrix by resolving the belts in ethanol under ultrasound. The PL spectrum of the purified nanobelts was recorded using a UV-lamp microzone Raman spectrometer under the excitation of a 325-nm HeCd laser at room temperature. The power output of the laser is 35 mW and the beam focus diameter is 2–5 μm. The PL of the amorphous matrix has also been measured for comparison.

3 Results and discussion

The morphologies of the heat-treated products were first examined using SEM. The low-magnification SEM images (Fig. 1a and b) show that white cotton-like nanofibers up to several mm in length were grown on the top of unreacted black-powder matrix. A typical tip of the nanobelts is shown as an inset picture in Fig. 1b. No droplets on the tips of the nanobelts were observed, implying that the vapor–liquid–solid (VLS) growth mechanism could not be dominant. A closer examination under high magnification (Fig. 1c and d) reveals that the cross sections of the nanostructures are rectangular with the thicknesses ranging from 20 to 40 nm and the widths from 400 to 600 nm, suggesting that the products possess nanobelt-like morphology. SEM images also reveal that, within each individual belt, the thickness and the width are uniform along its entire length, and the surfaces of the belts are smooth and clear without any residues. Figure 2 shows a typical XRD pattern of the synthesized nanobelts, suggesting that α-Si_3N_4 is the only crystalline phase. The broad hump at lower-angle regions suggests that the unreacted powders remain amorphous. It is estimated that about 15 wt. % of the original powders has been converted to the nanobelts.

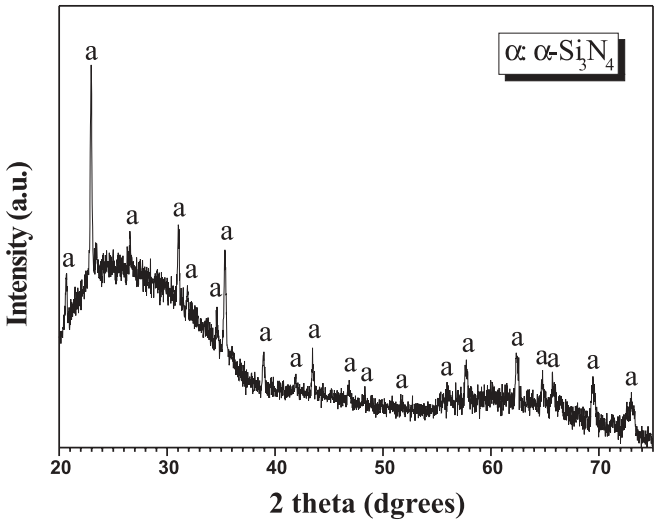

FIGURE 2 XRD pattern of as-pyrolyzed products suggests that α-Si_3N_4 is the only crystalline phase

Further characterization of the nanobelts was conducted using TEM and HRTEM. Figure 3a and b are the typical TEM images of the as-prepared nanobelts. The nanobelts are highly transparent, and the copper grid can even be seen through the thin nanobelts. The curved belts (shown as the inset picture in Fig. 3b) suggest the high flexibility of the as-synthesized nanostructures. The typical EDS result (inset

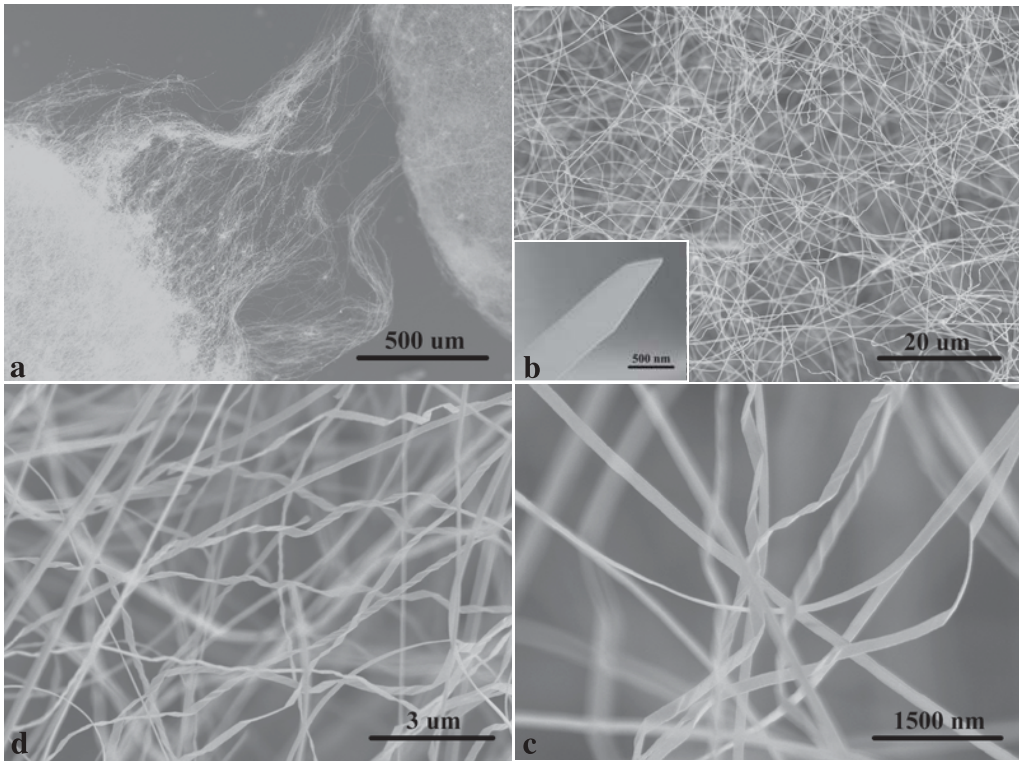

FIGURE 1 **a** and **b** show the ultra-long (up to several mm) nanobelt structure of Si_3N_4 synthesized at 1300 °C for 2 h under 0.1 MPa N_2, the *inset* in (**b**) shows a typical tip of the belts without any droplet; **c** and **b** are higher-magnification SEM images showing that the nanostructures possess a rectangular cross section. The surfaces of the belts are smooth and clear

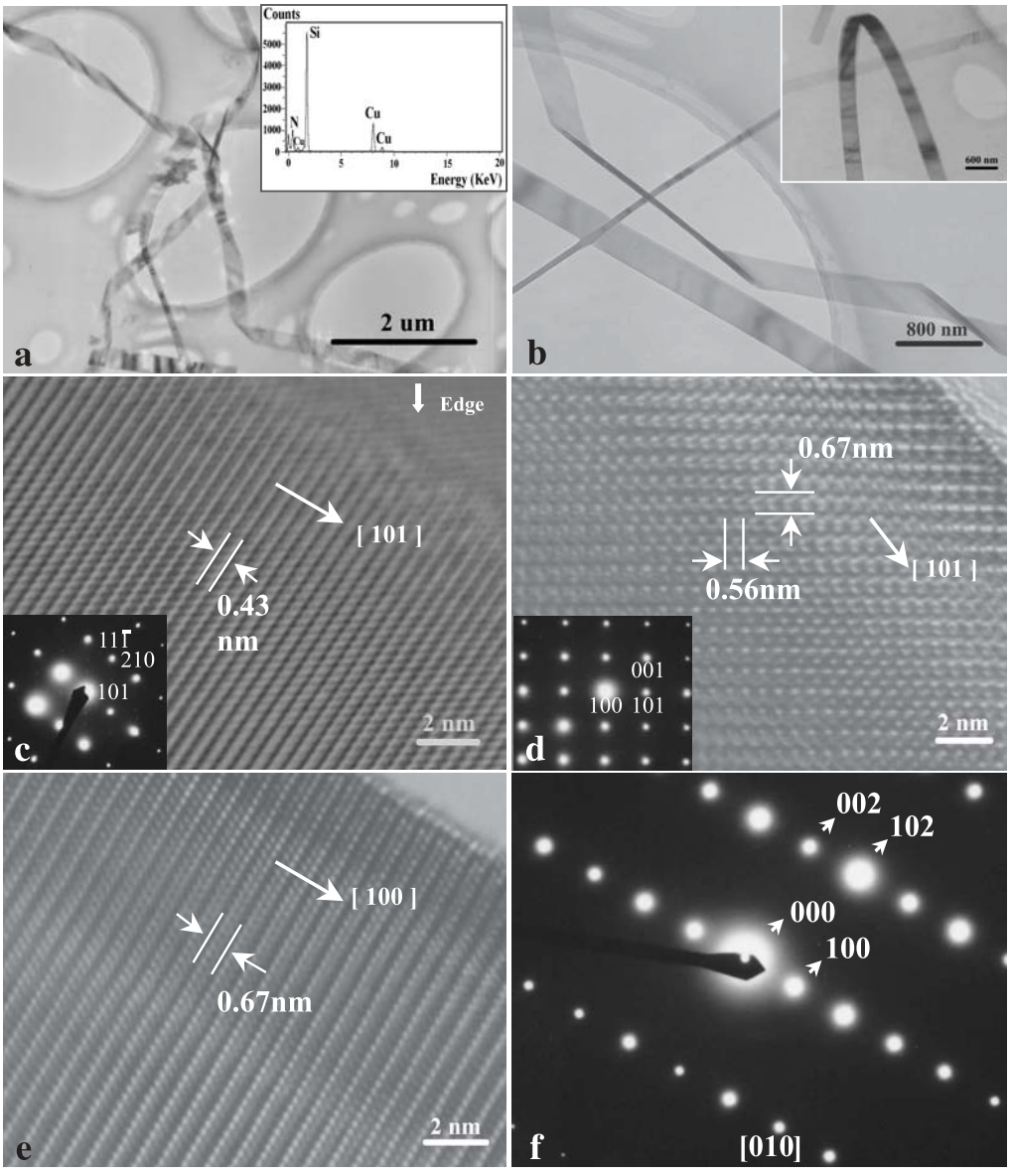

FIGURE 3 **a** and **b** typical TEM images of Si_3N_4 nanobelts. A typical EDS spectrum (*upper right inset* in (**a**)) shows that the nanobelts contain only Si and N elements. The curved nanobelt (*upper right inset* in (**b**)) suggests the high flexibility of the as-synthesized nanostructures. **c** HRTEM lattice image with the corresponding SAED pattern (*lower left inset* obtained from [$\bar{1}$21] zone axis) shows the growth direction of [101], **d** HRTEM lattice image with the corresponding SAED pattern (*lower left inset* obtained from [010] zone axis) shows the growth direction of [101], **e** HRTEM lattice image and corresponding SAED pattern (**f**) obtained from [010] zone axis show the growth direction of [100]. The measured *d* spacings of 0.43, 0.67 and 0.56 nm in (**c**)–(**e**) correspond to (101), (100) and (001) planes of α-Si_3N_4, respectively

in Fig. 3a) shows that the nanobelts contain only Si and N elements (Cu comes from the copper grid). Typical HRTEM images show that the α-Si_3N_4 nanobelts grew along different directions with inset SAED patterns obtained from the [-121] (3c) and [010] (3d and f) zone axes. The images reveal that the nanobelts contain few defects such as stacking faults and dislocations. SAED patterns are identical over the entire belt, indicating that the belt possesses a single-crystalline structure. The measured *d* spacings of 0.43, 0.67 and 0.56 nm are in good agreement with (101), (100) and (001) planes of bulk α-Si_3N_4, where $a = 0.77541$ nm and $c = 0.56217$ nm (JCPDS Card No. 41-0360). Both HRTEM images and SAED patterns suggest that [101] and [100] are growth directions for the α-Si_3N_4 nanobelts, as shown in Fig. 3c–f. The observations of more than 10 belts suggest that [101] and [100] are the only two growth directions for the nanobelts.

No nanobelts were formed in the samples without $FeCl_2$ additives, suggesting the catalytic growth of the α-Si_3N_4 in this study.

Generally, catalytic growth of the one-dimensional structures followed the vapor–liquid–solid growth mechanism that was first proposed by Wagner and Ellis [20]. A previous study [19] of the pyrolysis of pure Ceraset without the catalyst revealed that the polysilazane was converted to an amorphous alloy with an apparent composition of $SiC_{0.99}N_{0.84}$ at $\sim 1000\,^{\circ}C$ under 0.1 MPa N_2. This material remained predominantly amorphous up to $\sim 1450\,^{\circ}C$ where it crystallized to Si_3N_4 and free carbon. The Si_3N_4 and free carbon then reacted with each other to form SiC and N_2 gas at $\sim 1500\,^{\circ}C$ [19, 21]. These studies clearly suggested that the VLS mechanism was not valid in the current study simply because of the absence of Si-containing vapor phase during the pyrolysis. Considering these circumstances, we suggest a growth mechanism based on a combination of solid–liquid–solid (SLS) and gas–solid (GS) for the Si_3N_4 nanobelts. At the beginning of the process, the amorphous SiCN reacted with Fe to form a liquid Si−Fe−C alloy at a temperature higher than the eutectic temperature of the Si−Fe−C ternary system

(which is obviously lower than 1300 °C), meanwhile releasing N_2 gas. Further reaction of the SiCN and the liquid alloy formed a supersaturated liquid phase. This supersaturated liquid phase then reacted with N_2 gas to precipitate the Si_3N_4 nanobelts. The precipitation phase is silicon nitride rather than silicon or silicon carbide because under the pyrolysis conditions, namely 1300 °C and 0.1 MPa N_2, the silicon nitride is the most stable phase [21]. The formation of high-energy α-phase, instead of more stable β-phase, is due to the combination of the SLS-GS growth mechanisms [22, 23]. The mechanism that governed the formation of belt-like morphology in the current study is rather difficult to understand; particularly it has been reported [4] that α-Si_3N_4 nanowires with cross sections close to a circle were formed under similar growth conditions at 1200 °C. It was believed that the formation of the belt-like cross section is due to the anisotropic growth at earlier stages of growth, in which the growth rate along the width direction is much higher than that along the thickness direction. Previous studies [24, 25] suggested that the difference in growth rates of Si_3N_4 along different crystalline directions can be up to 100 times. The growths along the width/thickness directions stopped after they reached certain values limited by the confining effect of the liquid-phase droplets and further growth only occurred along the axial direction to form nanobelts. A detailed study of the effect of crystalline orientation on anisotropic growth in nanostructures is ongoing. Accordingly, it is believed that the formation of nanowires instead of nanobelts in [4] was because the liquid droplets formed at lower temperatures are small and limit the anisotropic growth at an earlier stage. The temperature dependence of the size of the liquid droplets can be understood by the fact that at higher temperatures more silicon (carbon) can be dissolved in equilibrium liquid phase. Another possibility is that the higher temperature favors the anisotropic growth. Investigation of this issue is ongoing and will be reported separately.

The optical emission of the nanobelts was measured using the 325-nm line of a HeCd laser as excitation source. The nanobelts exhibited intensive luminescence that can even be seen by the naked eye. Figure 4 shows a typical PL spectrum of the nanobelts obtained at room temperature. A similar measurement on the matrix amorphous SiCN particles fails to record any light emission, suggesting that the PL spectrum is from the nanobelts. The spectrum is slightly different from that reported previously [8]. A broad peak ranges from 1.5 to 3.5 eV with a maximum centered at 2.4 eV and two shoulders centered at 1.8 and 3 eV, respectively. Similar emission properties were also observed in amorphous silicon nitride films [26–30]. Robertson [31, 32] has defined defects in silicon nitride to be of four types, namely, Si−Si, N−N and Si and N dangling bonds. The Si−Si bond forms a σ state near the valence band and an empty σ^* state close to the conduction band. These two states forms the optical band edges. The Si dangling bond between N_3 and Si (referred as to a K center) forms a state about the mid gap, while the N dangling bond between Si_2 and N (referred as to an N center) forms two defect states that have been calculated to be near the conduction and the valence band, respectively. The K center forms a dominant trap and recombination center in silicon nitride and participates in the radiation transitions giving rise to the luminescence. The current PL result can be explained according to Robertson's modul by assuming Si−Si (σ–σ^*) bonds separated by 4.6 eV, as proposed by Pundur et al. [27]. The strong emission around 2.4 eV arises from recombination processes at the silicon dangling bond ($4.6/2 \pm 0.1 = 2.2$–2.4 eV). The weak emission at 1.8 eV can be attributed to recombination between two N dangling bonds. Finally, the emission at 3.0 eV is due to recombination either from the conduction band to the N_2^0 level or from the valence band to the N_4^+ level.

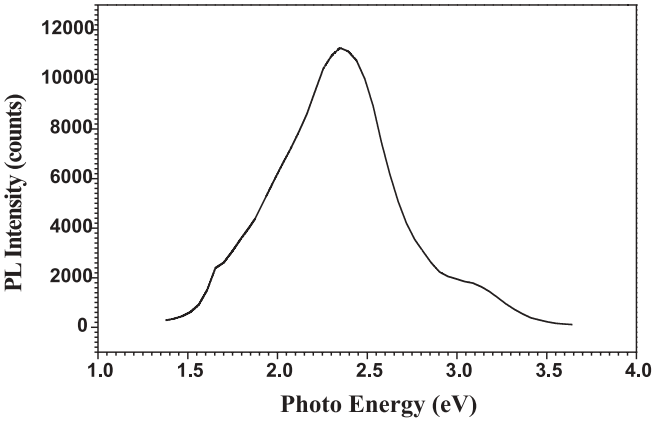

FIGURE 4 Photoluminescence of the Si_3N_4 nanobelts stacked on silicon wafer under excitation of 325-nm HeCd laser at room temperature

4 Conclusions

In summary, single-phase ultra-long single-crystalline α-Si_3N_4 nanobelts have been synthesized via a novel catalyst-assisted crystallization of polymer-derived amorphous SiCN at 1300 °C in 0.1 MPa N_2. The nanobelts are 20 to 40 nm in thickness and 400 to 600 nm in width and can grow up to several millimeters in length. The growth direction of the Si_3N_4 nanobelts can be either [101] or [100]. The growth mechanism is a combination of solid–liquid–solid and gas–solid reaction/crystallization. The formation of nanobelts instead of nanowires in this study is due to the anisotropic growth of Si_3N_4 nuclei at an earlier growth stage. Intensive light emission was observed between 1.5 and 3.5 eV with a maximum centered at 2.4 eV and two shoulders centered at 1.8 and 3 eV, respectively. The PL behavior is attributed to inherent defects in silicon nitride.

ACKNOWLEDGEMENTS This work is financially supported by the National Natural Science Foundation of China (Grant No. 50372031) and the 'Hundred Person' program of the Chinese Academy of Science.

REFERENCES

1 W. Han, S. Fan, Q. Li, B. Qu, D. Yu: Appl. Phys. Lett. **71**, 2271 (1997)
2 X. Wu, W. Song, B. Zhao, W. Huang, M. Pu, Y. Sun, J. Du: Solid State Commun. **115**, 683 (2000)
3 Y. Zhang, N. Wang, R. He, J. Liu, X. Zhang, J. Zhu: J. Cryst. Growth **233**, 803 (2001)
4 H. Kim, J. Park, H. Yang: Chem. Phys. Lett. **372**, 269 (2003)
5 H. Chen, Y. Cao, X. Xiang, J. Li, C. Ge: J. Cryst. Growth **325**, L1 (2001)
6 Y. Zhang, N. Wang, R. He, Q. Zhang, J. Zhu, Y. Yan: J. Mater. Res. **15**, 1048 (2000)
7 Y. Chen, L. Guo, D. Shaw: J. Cryst. Growth **210**, 527 (2000)

8 L. Yin, Y. Bando, Y. Zhu, Y. Li: Appl. Phys. Lett. **83**, 3584 (2003)
9 J. Hu, Y. Bando, T. Sekiguchi, F.F. Xu, J.H. Zhan: Appl. Phys. Lett. **84**, 804 (2004)
10 J. Hu, Y. Bando, Z. Liu, F. Xu, T. Sekiguchi, J. Zhu: Chem. Eur. J. **10**, 554 (2004)
11 F. Munakata, K. Matsuo, K. Furuya, Y. Akimune, J. Ye, I. Ishikawa: Appl. Phys. Lett. **74**, 3498 (1999)
12 A.R. Zanatta, L.A.O. Nunes: Appl. Phys. Lett. **72**, 3127 (1998)
13 F. Giorgis: Appl. Phys. Lett. **77**, 522 (2000)
14 A. Aydinli, A. Serpenguzel, D. Vardar: Solid State Commun. **98**, 273 (1996)
15 M. Molinari, H. Rinnert, M. Vergnat: Appl. Phys. Lett. **77**, 3499 (2000)
16 W. Yang, H. Miao, Z. Xie, L. Zhang, L. An: Chem. Phys. Lett. **383**, 441 (2004)
17 W. Yang, Z. Xie, H. Miao, H. Ji, L. Zhang, L. An: J. Am. Ceram. Soc. (2004) accepted
18 W. Yang, Z. Xie, J. Li, H. Miao, L. Zhang, H. Ji, L. An: J. Cryst. Growth (2004) accepted
19 Y. Li, E. Kroke, R. Riedel, C. Fasel, C. Gervais, F. Babonneau: Appl. Organometal. Chem. **15**, 820 (2001)
20 R.S. Wagner, W.C. Ellis: Appl. Phys. Lett. **4**, 89 (1964)
21 H.J. Seifert, J. Peng, H.L. Lucas, F. Aldinger: J. Alloys Compd. **320**, 251 (2001)
22 C.M.B. Henderson, D. Taylor: Trans. Br. Ceram. Soc. **74**, 49 (1975)
23 K. Blegen: Spec. Ceram. **6**, 223 (1975)
24 C. Hwang, T. Tian: Mater. Sci. Forum **47**, 285 (1989)
25 M. Kramer, M.J. Hoffmann, G. Petzow: J. Am. Ceram. Soc. **76**, 2778 (1993)
26 L.G. Austin, W.A. Jackson, T.M. Searle, P.K. Bhat, R.A. Gibson: Philos. Mag. B **52**, 271 (1985)
27 A.P. Pundur, J.G. Shavalgin, V.A. Gritsenko: Phys. Status Solidi A **95**, K107 (1986)
28 V.V. Vasilev, I.P. Mikhailovskii, K.K. Svitashev: Phys. Status Solidi A **95**, K37 (1986)
29 V.A. Nadolinny, V.V. Vasilev, I.P. Mikhailovskii: Phys. Status Solidi A **116**, K105 (1989)
30 C. Savall, E. Bustarret, J.P. Stoquert, J.C. Bruyere: Mater. Res. Soc. Symp. Proc. **284**, 77 (1993)
31 J. Robertson: Philos. Mag. B **63**, 47 (1991)
32 J. Robertson: Mater. Res. Soc. Symp. Proc. **284**, 65 (1993)